

Formation mechanism, thermal and magnetic properties of $(\text{Bi}_{1-x}\text{Sr}_x)_{m+1}\text{Fe}_{m-3}\text{Ti}_3\text{O}_{3(m+1)-\delta}$ ($m = 4 - 7$) ceramics

N. A. Lomanova¹, M. V. Tomkovich¹, V. L. Ugolkov², M. P. Volkov¹, I. V. Pleshakov¹,
V. V. Panchuk^{3,4}, V. G. Semenov^{3,4}

¹Ioffe Institute, 26 Polytekhnicheskaya Str., St. Petersburg
194021, Russian Federation

²Grebenshchikov Institute of Silicates Chemistry RAS, Adm. Makarova emb. 2, St. Petersburg,
199034, Russian Federation

³St. Petersburg State University, 7-9 Universitetskaya Emb., St. Petersburg, 199034, Russian Federation

⁴Institute for Analytical Instrumentation of RAS, St. Petersburg, ul. Ivana Chernykh, 31-33, lit. A.,
198095, Russian Federation
natus@mail.ioffe.ru

DOI 10.17586/2220-8054-2018-9-5-676-687

Specific features of the formation of Aurivillius phases $(\text{Bi}_{1-x}\text{Sr}_x)_{m+1}\text{Fe}_{m-3}\text{Ti}_3\text{O}_{3(m+1)-\delta}$ ($m = 4 - 7$; $x = 0.0 - 0.7$) with a perovskite-like block having a nanometric thickness (h) of 2 – 3 nm are described. It has been established that the degree of isomorphous substitution in the bismuth sublattice and thermal stability of phases tend to reduce with the increasing h . It has been demonstrated that the magnetic ions inside the perovskite-like block can have antiferromagnetic interaction exchange that influences magnetic properties of the Aurivillius phases.

Keywords: aurivillius phases, nanolayers, perovskite-like nanoblocks, formation mechanism, thermal properties, magnetic properties.

Received: 21 August 2018

Revised: 26 September 2018

1. Introduction

The search for and design of new perovskite-like multiferroics is a promising trend in material science, as media possessing both ferroelectric and magnetic order are among the most highly demanded materials in modern technology [1–4]. The interest in layered Aurivillius phase multiferroics is determined by the possibility of the nanolayers' structural stabilization during the formation of those nanostructured materials [5, 6].

In general, the structures of the layered perovskite-like oxides such as the Aurivillius phases $\text{Bi}_{m+1}\text{Fe}_{m-3}\text{Ti}_3\text{O}_{3m+3}$ consist of alternating fluorite-like $\{(\text{Bi}_2\text{O}_2)^{2+}\}_\infty$ nanolayers and bismuth orthoferrite-based perovskite-like blocks of $\{(\text{Bi}_{m+1}\text{Fe}_{m-3}\text{Ti}_3\text{O}_{3m+1})^{2-}\}_\infty$ [7]. The thickness h of the perovskite-like blocks differs depending on the number of nanolayers m .

Bismuth orthoferrite-based (BiFeO_3) materials are known to have high values of the Neel temperature ($T_N \approx 370$ °C) and the Curie point ($T_C \approx 830$ °C), and currently have very attractive properties from a magnetoelectronics point of view. The main interest in the design of the Aurivillius phase-structured materials is also associated with the possibility of controlling their functional properties by varying the composition and thickness of the perovskite-like blocks up to nanometric values [1–6, 8–23]. In the Aurivillius phases with $m=7-9$, the perovskite-like block has a thickness of 3 – 4 nm [5].

In a unit cell of $\text{Bi}_{m+1}\text{Fe}_{m-3}\text{Ti}_3\text{O}_{3m+3}$, titanium and iron ions have octahedral structurally nonequivalent positions in the inner and outer layers of a perovskite-like block. It is shown in [6, 9–17] that the distribution of cations within a perovskite-like block depends on m and may affect stability and properties of the Aurivillius phases. In particular, it can influence the conductivity of these compounds and their magnetic behavior [13, 14, 17].

The Aurivillius phases' thermal behavior, phase equilibria and transformations in binary and quasi-binary sections of the $\text{Bi}_2\text{O}_3\text{--SrO--TiO}_2\text{--Fe}_2\text{O}_3$ system were studied in [10, 17–21]. It was demonstrated for the non-doped Aurivillius phases $\text{Bi}_{m+1}\text{Fe}_{m-3}\text{Ti}_3\text{O}_{3m+3}$ that an increase in the perovskite-like block thickness up to the nanosize values leads to a decrease in their thermal stability. The Aurivillius phases $\text{Bi}_{m+1}\text{Fe}_{m-3}\text{Ti}_3\text{O}_{3m+3}$ have the values of the temperature of transition to the magnetically ordered state (Neel point, T_N) within the 77–360 K range, and the ferroelectric transition temperature (Curie point, T_C) within the range of 923 – 1023 K [11, 14, 15, 17, 21–26]. Along with that, magnetic ordering may be expected around room temperature in substances with $h \geq 3$ ($m \geq 7$) [14]. Above T_C (923–1023 K), the structures of the Aurivillius phases $\text{Bi}_{m+1}\text{Fe}_{m-3}\text{Ti}_3\text{O}_{3m+3}$ are tetragonal, while in the ferroelectric phase the crystal lattice is either orthorhombic or monoclinic [15, 24].

The influence of isomorphous substitution in the Aurivillius phase structures on their phase transition temperatures requires systematic study.

The methods of synthesizing simple bismuth-containing perovskites and layered perovskite-like oxides, which make it possible to perform the synthesis of materials while varying their morphology and particle sizes within a broad range by changing technological parameters, are described, for example, in [27–40]. It is shown that irrespective of the technology, material formation begins at the melting temperature of the surface (non-autonomous) bismuth oxide-based phase, at which mass transfer in the reaction system is activated [41–43]. A study of the formation of phases with variable composition during the isomorphous substitution of ions in the Aurivillius phases structure requires refining of the mechanism of phase formation.

The present work offers a study of the formation processes, as well as of thermal and magnetic properties of ceramic materials based on the Aurivillius phases $(\text{Bi}_{1-x}\text{Sr}_x)_{m+1}\text{Fe}_{m-3}\text{Ti}_3\text{O}_{3(m+1)-\delta}$ with different degrees of isomorphous substitution for strontium in the bismuth sublattice.

2. Experimental

The method of solid-phase chemical reactions was used for producing samples with a nominal composition corresponding to $(\text{Bi}_{1-x}\text{Sr}_x)_{m+1}\text{Fe}_{m-3}\text{Ti}_3\text{O}_{3(m+1)-\delta}$ ($m = 4, 5, 6, 7$ and $x = 0.0 - 0.7$).

The reagents used were the bismuth oxide, iron(III) oxide, titanium oxide and strontium carbonate (all of the 99.9% purity).

The samples were heat treated in the “heating – isothermal exposure – cooling” mode. The isothermal exposure was performed from 500 – 1000 °C for 5 – 80 hours at each temperature, depending on the degree of synthesis completion. The phase composition of the samples at each stage of synthesis was determined by X-ray diffraction (XRD-7000 Shimadzu diffractometer, CuK_α -radiation). The unit cell parameters were calculated using the PDWin 4.0 software package.

The microstructure and elemental composition of the samples were determined by scanning electron microscopy and elemental energy-dispersive microanalysis (FEI Quanta 200 SEM with EDAX attachment). The chemical formula of the synthesized substance was calculated according to stoichiometry and based on the assumption that the oxidation states of Bi, Sr, Ti and Fe are III, II, IV and III, respectively. In order to determine the main phase, the sample area and individual smaller sites were subjected to the elemental analysis.

The samples' thermal behavior was studied by differential scanning calorimetry (DSC) using the NETZSCH STA 429 calorimeter, in air, with the heating rate of 10 °C/min. The changes in the samples' linear dimensions were determined by dilatometry using the NETZSCH DIL 402 E dilatometer, in air, with the heating rate of 10 °C/min. A pellet-shaped sample, 5 mm in diameter and 3 mm thick, was used. The linear thermal dilation coefficient (α_t) was determined within the 200 – 400 °C range, in which phase transformations are absent.

The Mössbauer spectroscopy of the samples was accomplished using the WISSEL spectrometer in the absorption geometry at room temperature, using a $^{57}\text{Co}(\text{Rh})$ source. The isomer shift values were determined with reference to the α -Fe isomer shift.

The samples' magnetic behavior was determined using a Physical Properties Measuring System, Quantum Design vibration magnetometer. Specific magnetization M as a function of temperature was studied in the presence of a constant field $H = 500$ Oe and in the zero field cooling (ZFC) mode. The $M(H)$ dependence was measured at 5 and 300 K within the 0 – 50 kOe range.

3. Results and discussion

The Aurivillius phase-structured solid solutions $(\text{Bi}_{1-x}\text{Sr}_x)_{m+1}\text{Fe}_{m-3}\text{Ti}_3\text{O}_{3(m+1)-\delta}$ have been synthesized in the Bi_2O_3 – SrO – TiO_2 – Fe_2O_3 system. The value of δ can vary depending on the charge compensation character during formation of the $(\text{Bi}_{1-x}\text{Sr}_x)_{m+1}\text{Fe}_{m-3}\text{Ti}_3\text{O}_{3(m+1)-\delta}$ solid solution. If the charge is compensated at the expense of the change in the iron ions charge from Fe^{3+} to Fe^{4+} , then $\delta = 0$, while in the case of oxygen vacancies creation $\delta = 0.5x(m + 1)$. The possible character of the charge compensation may be determined from the Mössbauer data given below.

As is shown in [19], the structure of the homologous series $(\text{Bi}_{1-x}\text{Sr}_x)_{m+1}\text{Fe}_{m-3}\text{Ti}_3\text{O}_{3(m+1)-\delta}$ contains a perovskite-like block with the number of nanolayers $m = 4 - 7$ and thickness h of about 2 – 3 nm. Along with that, the limit of isomorphous substitution of bismuth for strontium (x) depends on the perovskite-like block thickness h . The $x(m)$ and, correspondingly, $x(h)$ dependences are illustrated in Fig. 1. It can be noted that the substitution of bismuth for strontium in the Aurivillius phases with the given composition occurs at an m up to ~ 7 ($h \sim 3$ nm). In this case, the isomorphous capacity of the system decreases with increasing thickness of the perovskite-like block to a nanosize value, and this influences the formation mechanisms of these substances, as well as thermal

and magnetic properties of ceramic materials based on them. The experimental results presented below have been analyzed in comparison with the corresponding data on the features of the solid-phase synthesis, structure and properties of the non-doped Aurivillius phases $\text{Bi}_{m+1}\text{Fe}_{m-3}\text{Ti}_3\text{O}_{3(m+1)}$, described in [6, 10, 14, 17, 21]. Synthesis conditions, elemental and phase compositions of the obtained samples are presented in Table 1.

TABLE 1. Synthetic conditions and sample composition

No.	Nominal composition	m	Synthesis conditions	Composition of the Aurivillius phases $(\text{Bi}_{1-x}\text{Sr}_x)_{m+1}\text{Fe}_{m-3}\text{Ti}_3\text{O}_{3(m+1)-\delta}$ after EDS-analysis	m^*	Phase composition by XRD analysis
1	$\text{Bi}_5\text{FeTi}_3\text{O}_{15}$	4	900 °C, 5 h	$\text{Bi}_{5.1\pm 0.1}\text{Fe}_{1.2\pm 0.1}\text{Ti}_3\text{O}_{15.5\pm 0.3}$	4.1	A
1-1	$\text{Bi}_{4.9}\text{Sr}_{0.1}\text{FeTi}_3\text{O}_{14.75}$	4	900 °C, 10 h	$\text{Bi}_{5.3\pm 0.3}\text{Sr}_{0.2\pm 0.1}\text{Fe}_{1.2\pm 0.1}\text{Ti}_3\text{O}_{16.0\pm 0.3}$	4.3	A
1-2	$\text{Bi}_{4.7}\text{Sr}_{0.3}\text{FeTi}_3\text{O}_{14.25}$	4	1000 °C, 10 h	$\text{Bi}_{4.9\pm 0.2}\text{Sr}_{0.3\pm 0.2}\text{Fe}_{1.1\pm 0.3}\text{Ti}_3\text{O}_{15.3\pm 0.2}$	4.1	A
1-3	$\text{Bi}_{4.5}\text{Sr}_{0.5}\text{FeTi}_3\text{O}_{13.75}$	4	1000 °C, 10 h	$\text{Bi}_{4.7\pm 0.2}\text{Sr}_{0.4\pm 0.2}\text{Fe}_{1.3\pm 0.2}\text{Ti}_3\text{O}_{15.4\pm 0.2}$	4.2	A
1-4	$\text{Bi}_{4.3}\text{Sr}_{0.7}\text{FeTi}_3\text{O}_{13.25}$	4	1000 °C, 10 h	$\text{Bi}_{4.6\pm 0.1}\text{Sr}_{0.6\pm 0.1}\text{Fe}_{1.1\pm 0.2}\text{Ti}_3\text{O}_{15.2\pm 0.1}$	4.1	A
1-5	$\text{Bi}_{4.1}\text{Sr}_{0.9}\text{FeTi}_3\text{O}_{12.75}$	4	1000 °C, 10 h	$\text{Bi}_{3.9\pm 0.2}\text{Sr}_{1.2\pm 0.4}\text{Fe}_{1.2\pm 0.2}\text{Ti}_3\text{O}_{14.9\pm 0.1}$	4.1	A, P, M
2	$\text{Bi}_6\text{Fe}_2\text{Ti}_3\text{O}_{18}$	5	890 °C, 5 h	$\text{Bi}_{5.8\pm 0.2}\text{Fe}_{1.8\pm 0.2}\text{Ti}_3\text{O}_{17.4\pm 0.2}$	4.8	A
2-1	$\text{Bi}_{5.7}\text{Sr}_{0.3}\text{Fe}_2\text{Ti}_3\text{O}_{17.1}$	5	900 °C, 10 h	$\text{Bi}_{5.9\pm 0.2}\text{Sr}_{0.3\pm 0.1}\text{Fe}_{2.3\pm 0.1}\text{Ti}_3\text{O}_{18.6\pm 0.2}$	5.2	A, M
3	$\text{Bi}_7\text{Fe}_3\text{Ti}_3\text{O}_{21}$	6	870 °C, 5 h	$\text{Bi}_{7.4\pm 0.3}\text{Fe}_{3.0\pm 0.2}\text{Ti}_3\text{O}_{21.6\pm 0.2}$	6.3	A
3-1	$\text{Bi}_{6.7}\text{Sr}_{0.3}\text{Fe}_3\text{Ti}_3\text{O}_{19.95}$	6	900 °C, 20 h	$\text{Bi}_{6.8\pm 0.2}\text{Sr}_{0.4\pm 0.1}\text{Fe}_{3.2\pm 0.2}\text{Ti}_3\text{O}_{21.4\pm 0.3}$	6.2	A, M, S
4	$\text{Bi}_8\text{Fe}_4\text{Ti}_3\text{O}_{24}$	7	870 °C, 5 h	$\text{Bi}_{8.0\pm 0.1}\text{Fe}_{4.2\pm 0.2}\text{Ti}_3\text{O}_{24.3\pm 0.3}$	7.1	A, M
4-1	$\text{Bi}_{7.7}\text{Sr}_{0.3}\text{Fe}_4\text{Ti}_3\text{O}_{22.8}$	7	900 °C, 20 h	$\text{Bi}_{7.5\pm 0.1}\text{Sr}_{0.4\pm 0.1}\text{Fe}_{4.0\pm 0.2}\text{Ti}_3\text{O}_{23.7\pm 0.1}$	7.0	A, M
			870 °C, 10 h	$\text{Bi}_{6.5\pm 0.1}\text{Sr}_{0.4\pm 0.2}\text{Fe}_{2.2\pm 0.2}\text{Ti}_3\text{O}_{19.5\pm 0.3}$	5.5	A, P
				$\text{Bi}_{7.5\pm 0.1}\text{Sr}_{0.4\pm 0.1}\text{Fe}_{3.2\pm 0.1}\text{Ti}_3\text{O}_{22.5\pm 0.5}$	6.5	
				$\text{Bi}_{1.1\pm 0.1}\text{Sr}_{0.1\pm 0.1}\text{Fe}_{0.7\pm 0.1}\text{Ti}_{0.3}\text{O}_{3.4\pm 0.2}$	—	

*) average value from EDS- analysis. Notation: A – Aurivillius phases, P – BiFeO_3 , M – $\text{Bi}_2\text{Fe}_4\text{O}_9$, S – $\text{Bi}_{25}\text{FeO}_{39}$

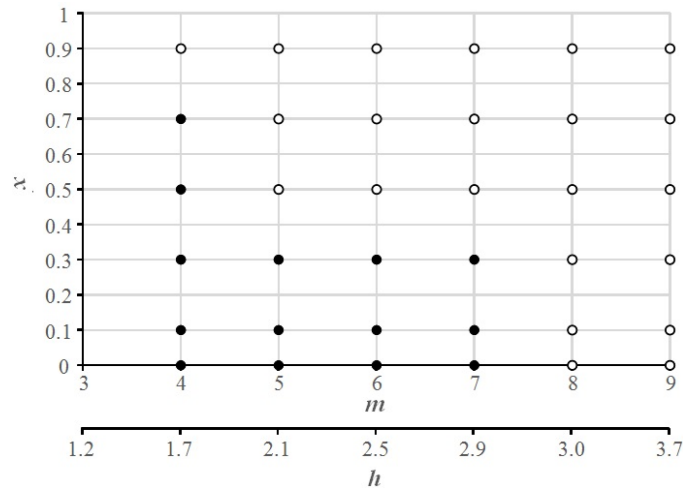


FIG. 1. Scheme for isomorphous substitution of bismuth by strontium in Aurivillius phases $(\text{Bi}_{1-x}\text{Sr}_x)_{m+1}\text{Fe}_{m-3}\text{Ti}_3\text{O}_{3(m+1)-\delta}$ structure

X-ray diffractograms of the Sr-doped Aurivillius phases $(\text{Bi}_{1-x}\text{Sr}_x)_{m+1}\text{Fe}_{m-3}\text{Ti}_3\text{O}_{3(m+1)-\delta}$, presented in Fig. 2 illustrate the phase composition of the samples at a synthesis stage from 500 – 1000 °C. At 500 – 600 °C, that is, after melting of the bismuth oxide-based surface phase [28, 33] and hence, after activation of mass transfer in the reaction system [41–43], $\alpha\text{-Bi}_2\text{O}_3$ interacts with titanium and iron oxides yielding the main phase $\text{Bi}_{25}\text{FeO}_{39}$.

At 700 °C, small amounts of BiFeO₃ and Aurivillius phases start to appear in the reaction system (Fig. 2). The sillenite-structured Bi₂₅FeO₃₉ and perovskite-structured BiFeO₃ are the intermediate products in the synthesis of the Aurivillius phases. Their formation in the reaction system facilitates the formation of a layered perovskite-like structure with a predetermined composition due to a gradual rearrangement in the first coordination sphere of bismuth [28]. According to the quantitative X-ray phase analysis, the share of BiFeO₃ increases along with the increasing Sr content in the reaction system, and with the increasing *h*. At temperatures above the initiation of Bi₂₅FeO₃₉ decomposition (above 700 °C), diffractograms of the samples with *m* = 4 show reflexes of only Aurivillius phases and BiFeO₃, their ratio being the evidence of the gradual formation of a layered perovskite-like structure. Formation of the target product occurs at temperatures above that of metastable BiFeO₃ decomposition (855±5 °C [39]).

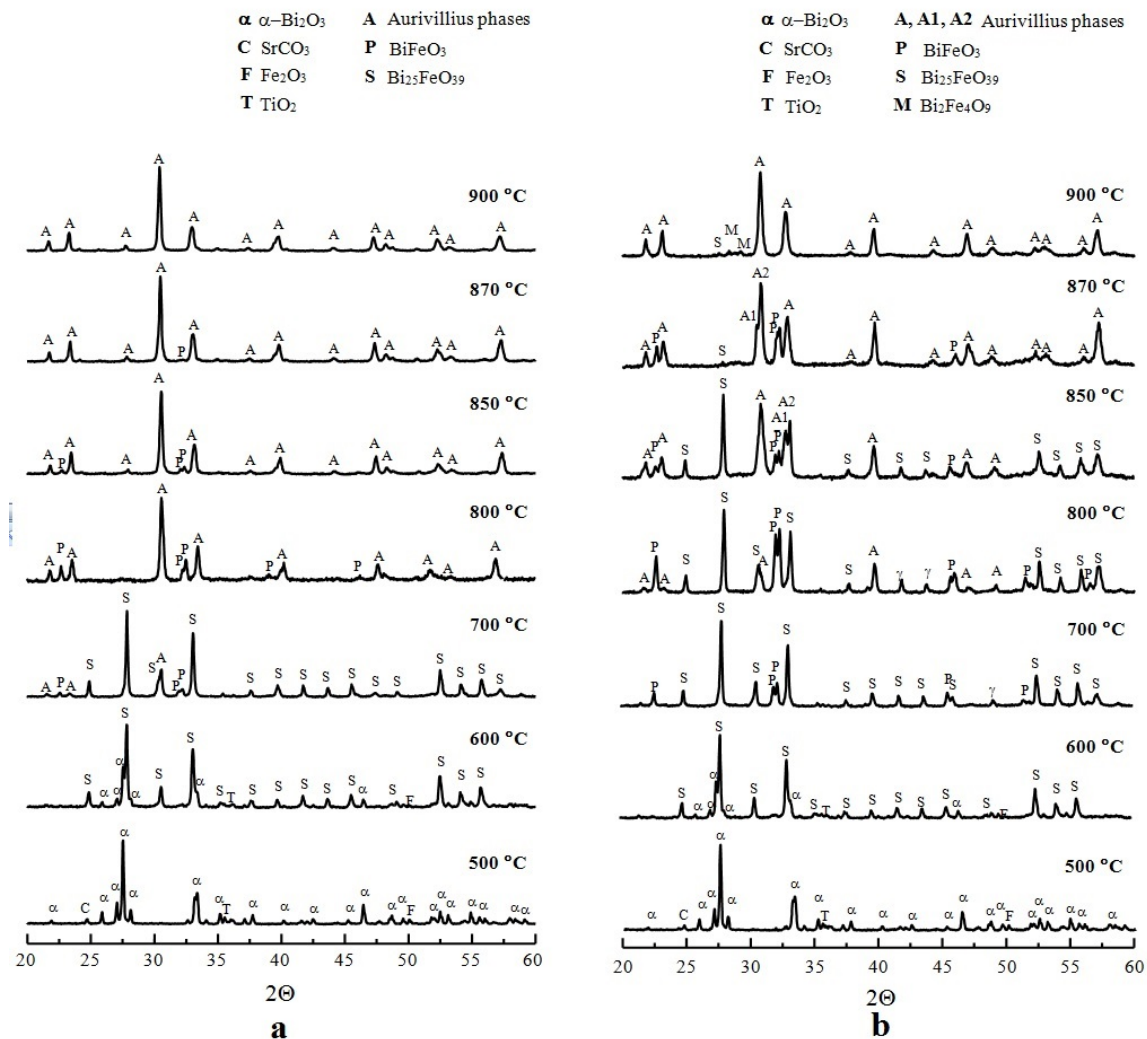


FIG. 2. X-ray diffractograms ($\lambda = 1.54056 \text{ \AA}$) of $(\text{Bi}_{1-x}\text{Sr}_x)_{m+1}\text{Fe}_{m-3}\text{Ti}_3\text{O}_{3(m+1)-\delta}$ after thermal treatment at 500, 600, 700, 800, 850, 870 and 900 °C: a – $\text{Bi}_{4.7}\text{Sr}_{0.3}\text{FeTi}_3\text{O}_{15-\delta}$ ($m = 4$); b – $\text{Bi}_{6.7}\text{Sr}_{0.3}\text{Fe}_3\text{Ti}_3\text{O}_{21-\delta}$ ($m = 7$)

Diffractograms of the multilayered Aurivillius phases with $m > 5$ ($h > 2.5 \text{ nm}$) show that the process of Bi₂₅FeO₃₉ decomposition proceeds gradually up to 850 °C, and the substance of this phase is spent to increase the share of BiFeO₃ in the reaction system. At 870 °C, the diffractogram of a $\text{Bi}_{7.7}\text{Sr}_{0.3}\text{Fe}_4\text{Ti}_3\text{O}_{24-\delta}$ sample with $m = 7$ shows that the two main products are $(\text{Bi}_{1-x}\text{Sr}_x)_{m+1}\text{Fe}_{m-3}\text{Ti}_3\text{O}_{3(m+1)-\delta}$ and the perovskite-like BiFeO₃. It should be noted that the reflexes observed at the intermediate stages of synthesis correspond to the Aurivillius phases with a smaller *m*, which is confirmed by the elemental analysis for the sample with $m = 7$, heat treated at 870 °C (Table 1).

When the temperature is further increased, the perovskite-like BiFeO_3 builds into the layered structure, and it leads to the formation of the target product $(\text{Bi}_{7.3}\text{Sr}_{0.3}\text{Fe}_4\text{Ti}_3\text{O}_{24-\delta})$ with an output around 95%. Some quantity of the impurity phases on the basis of $\text{Bi}_{25}\text{FeO}_{39}$, and $\text{Bi}_2\text{Fe}_4\text{O}_9$ resulting from its decomposition, are observed at the final stages of $(\text{Bi}_{1-x}\text{Sr}_x)_{m+1}\text{Fe}_{m-3}\text{Ti}_3\text{O}_{3(m+1)-\delta}$ synthesis. Their quantity is increasing along with the number of layers m and, hence thickness of the nano-sized perovskite-like block. In contrast to the Sr-doped Aurivillius phases, the $\text{Bi}_{m+1}\text{Fe}_{m-3}\text{Ti}_3\text{O}_{3(m+1)}$ homologous series can have a higher degree of homogeneity, having been synthesized at a lower temperature and a shorter isothermal exposure (see Table 1).

X-ray diffractograms of the obtained materials with the phase and elemental composition corresponding to the target product output of over 90 % (see Table 1) are presented in Fig. 3(a,b). It may be noted that the Sr-doped Aurivillius phases with $m > 5$ perovskite-like layers contain a small number of impurity phases (Fig. 3b). The data on the orthorhombic unit cell volume (Table 2) suggest that it poorly depends on the isomorphous substitution in the structure and increases with the increasing m .

TABLE 2. Sample characteristics

No	Samples	m	V^* , Å^3	T_K , °C	T_{dec} , °C	T_S , °C	α_t , 1/K	M_s , emu/g, at 20kOe
1	$\text{Bi}_5\text{FeTi}_3\text{O}_{15}$	4	1226	740 [7, 23]	1100	840 [7, 20, 21]	10 [21]	0.10
1-1	$\text{Bi}_{4.9}\text{Sr}_{0.1}\text{FeTi}_3\text{O}_{15-\delta}$	4	1224	740	1050	770	9	—
1-2	$\text{Bi}_{4.7}\text{Sr}_{0.3}\text{FeTi}_3\text{O}_{15-\delta}$	4	1222	710 [7]	1080	765	10	0.10
1-3	$\text{Bi}_{4.5}\text{Sr}_{0.5}\text{FeTi}_3\text{O}_{15-\delta}$	4	1218	700	1130	700	8	0.10
1-4	$\text{Bi}_{4.3}\text{Sr}_{0.7}\text{FeTi}_3\text{O}_{15-\delta}$	4	1213	—	1150	650	9	0.11
2	$\text{Bi}_6\text{Fe}_2\text{Ti}_3\text{O}_{18}$	5	1520	690 [7, 23]	980 [7, 20, 21]	720 [7, 20, 21]	13 [21]	—
2-1	$\text{Bi}_{5.3}\text{Sr}_{0.3}\text{Fe}_2\text{Ti}_3\text{O}_{18-\delta}$	5	1516	625 [19]	900 [19]	680	10	0.13
3	$\text{Bi}_7\text{Fe}_3\text{Ti}_3\text{O}_{21}$	6	1710	682 [7]	980 [7, 20, 21]	635 [7, 20, 21]	11 [21]	0.13 [14]
3-1	$\text{Bi}_{6.7}\text{Sr}_{0.3}\text{Fe}_3\text{Ti}_3\text{O}_{21-\delta}$	6	1708	620 [19]	940 [19]	660	8	—
4	$\text{Bi}_8\text{Fe}_4\text{Ti}_3\text{O}_{24}$	7	1978	665 [7]	970 [7, 21]	765 [7, 20, 21]	12 [21]	0.15 [14]
4-1	$\text{Bi}_{7.3}\text{Sr}_{0.3}\text{Fe}_4\text{Ti}_3\text{O}_{24-\delta}$	7	1965	590 [19]	935 [19]	590	10	0.14

Typical SEM images of the samples after the final stage of heat treatment (Fig. 4) show the lamellar morphology of the resulting ceramic materials. The elemental chemical analysis data show that the main phase in the samples at the final stage of synthesis corresponds to the target product sufficiently well (Table 1). In order to refine the mechanism of formation of the layered perovskite-like structure, the composition of the $\text{Bi}_{7.3}\text{Sr}_{0.3}\text{Fe}_4\text{Ti}_3\text{O}_{24-\delta}$ sample ($m = 7$) was analyzed in more detail at the intermediate stage of synthesis. According to the obtained result, at 870 °C the sample contains the Aurivillius phases $(\text{Bi}_{0.6}\text{Sr}_{0.4})_{m+1}\text{Fe}_{m-3}\text{Ti}_3\text{O}_{3(m+1)-\delta}$ with $m < 7$, that is, with a smaller m value than that specified by stoichiometry (Table 1). Along with these phases, the bismuth orthoferrite-based solid solution $\text{Bi}_{1.1}\text{Sr}_{0.1}\text{Fe}_{0.7}\text{Ti}_{0.3}\text{O}_{2.7}$ is recorded. Under further thermal treatment, a part of its substance is used in the Aurivillius phase formation, while another part is engaged in formation of a mullite-like impurity phase $\text{Bi}_{2-x}\text{Sr}_x\text{Fe}_4\text{O}_{9-x}$. The small quantity of this phase prevents precise determination of its composition. However, it was shown in [19] that increasing the quantity of the impurity in the system, along with the increase in m and the limited solubility of $(\text{Bi}_{1-x}\text{Sr}_x)_{m+1}\text{Fe}_{m-3}\text{Ti}_3\text{O}_{3(m+1)-\delta}$, allowed a suggestion that one of the factors that complicates synthesis of the multilayered Sr-doped Aurivillius phases is the structural stabilization of impurity phases under isomorphous substitution in the bismuth sublattice.

Figure 5 and Table 2 present the results of the Sr-doped Aurivillius phase's thermal analysis. The influence of the isomorphous substitution in the bismuth sublattice on the thermal behavior of $(\text{Bi}_{1-x}\text{Sr}_x)_{m+1}\text{Fe}_{m-3}\text{Ti}_3\text{O}_{3(m+1)-\delta}$ has been considered for the first time in [19] for the fixed x value of 0.3. It was shown that such a degree of substitution makes the Curie point lower if compared with that for the non-doped Aurivillius phases, and the temperature of their decomposition insignificantly higher (see Table 2). The influence of isomorphous substitution on phase transformations and on the decomposition temperature has been studied for the four-layered Sr-doped Aurivillius phase $\text{Bi}_{5-x}\text{Sr}_x\text{FeTi}_3\text{O}_{15-\delta}$ ($x = 0.0, 0.3, 0.5, 0.7$), because this material shows the maximum degree of isomorphous substitution in the bismuth sublattice (see Fig. 5a).

The DSC curves for the $\text{Bi}_{5-x}\text{Sr}_x\text{FeTi}_3\text{O}_{15-\delta}$ samples show small endothermal effects in the medium temperatures domain ($T_C = 650 - 750$ °C, which correspond to a phase transition of the second kind from orthorhombic symmetry to tetragonal symmetry (Curie point) [22, 24]. Thermal effects in the high temperature domain

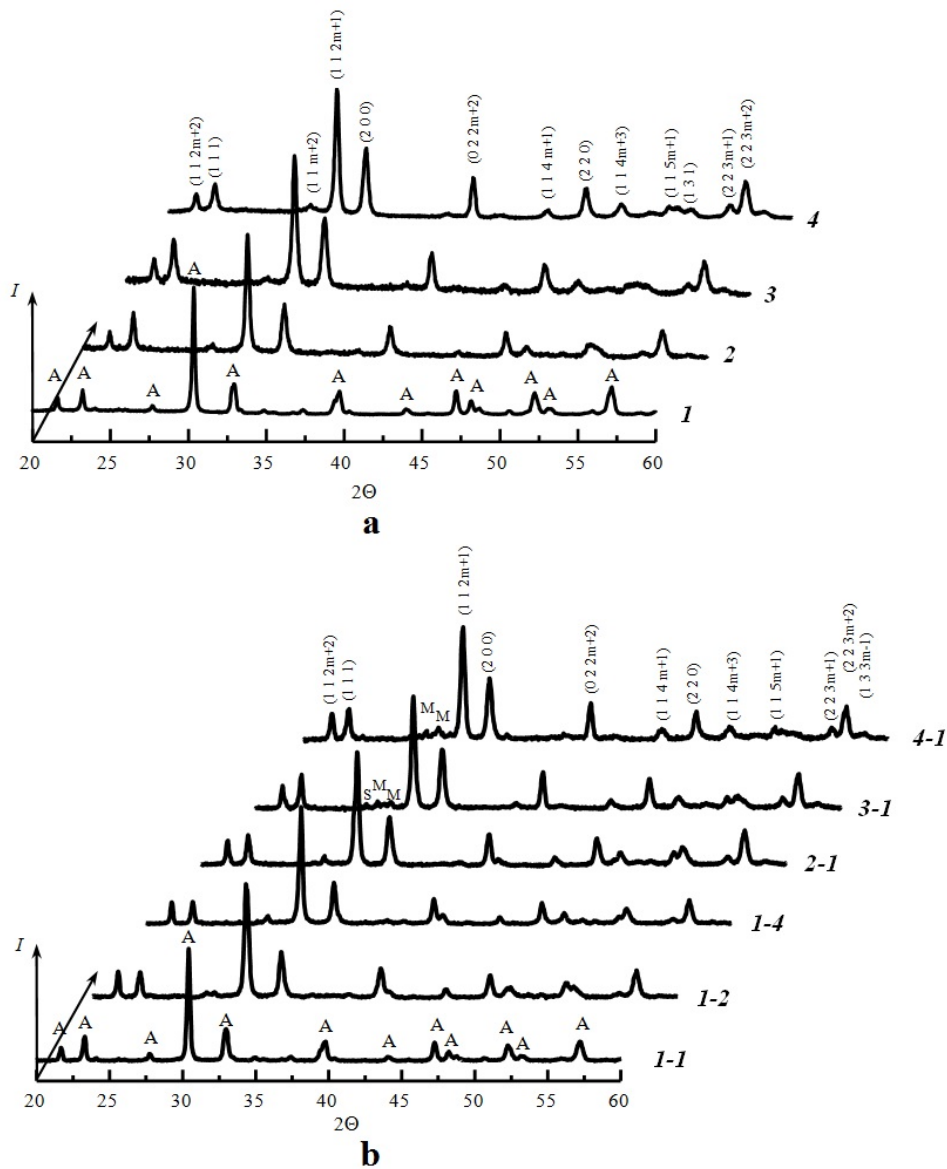


FIG. 3. X-ray diffractograms ($\lambda = 1.54056 \text{ \AA}$) of $(\text{Bi}_{1-x}\text{Sr}_x)_{m+1}\text{Fe}_{m-3}\text{Ti}_3\text{O}_{3(m+1)-\delta}$ after thermal treatment at 900°C : a – un-doped samples; b – Sr-doped samples. The curve number corresponds to the sample number (Table 1). Notation: A – Aurivillius phases, P – BiFeO_3 , M – $\text{Bi}_2\text{Fe}_4\text{O}_9$, S – $\text{Bi}_{25}\text{FeO}_{39}$

($T_{dec} > 900^\circ\text{C}$) are related to the Aurivillius phase decomposition [10, 18, 20, 21]. As can be seen, a peak at $740 \pm 5^\circ\text{C}$ is well-expressed for the non-doped sample $\text{Bi}_{5-x}\text{Sr}_x\text{FeTi}_3\text{O}_{15-\delta}$ ($x = 0.0$). For the Sr-doped Aurivillius phase, thermal effects at the Curie point are more diffuse. Along with that, no significant difference is observed for the T_C value in the case of bismuth ion substitution with a larger-radius ion ($r_{\text{Bi}^{3+}(\text{VIII})} = 1.25 \text{ \AA}$, $r_{\text{Sr}^{2+}(\text{VIII})} = 1.39 \text{ \AA}$ [44]). It follows from the analysis of high-temperature effects in DSC curves at different x values, that T_{dec} gradually grows together with the increasing degree of bismuth substitution with Sr, and in fact does not depend on thickness of the perovskite-like block at $m > 5$.

The curves of the Sr-doped Aurivillius phases' thermal expansion $dL/L_0(T)$ are presented in Fig. 5b. The sintering initiation temperature (T_S), was determined from the maximum of the $dL/L_0(T)$ curves. It lies within the $590 - 765^\circ\text{C}$ interval and tends to decrease with fewer fusible components in the system, that is, of bismuth and strontium oxides which localize on the grains' surface, as a rule. As is seen from Table 2, there is a correlation between T_S and T_C , which apparently suggests the activation of diffusion in the reaction system during a structural transition. The coefficient of linear thermal expansion of the obtained materials is $\alpha_t = 9 \pm 1 \cdot 10^{-6} \text{ K}^{-1}$ (see

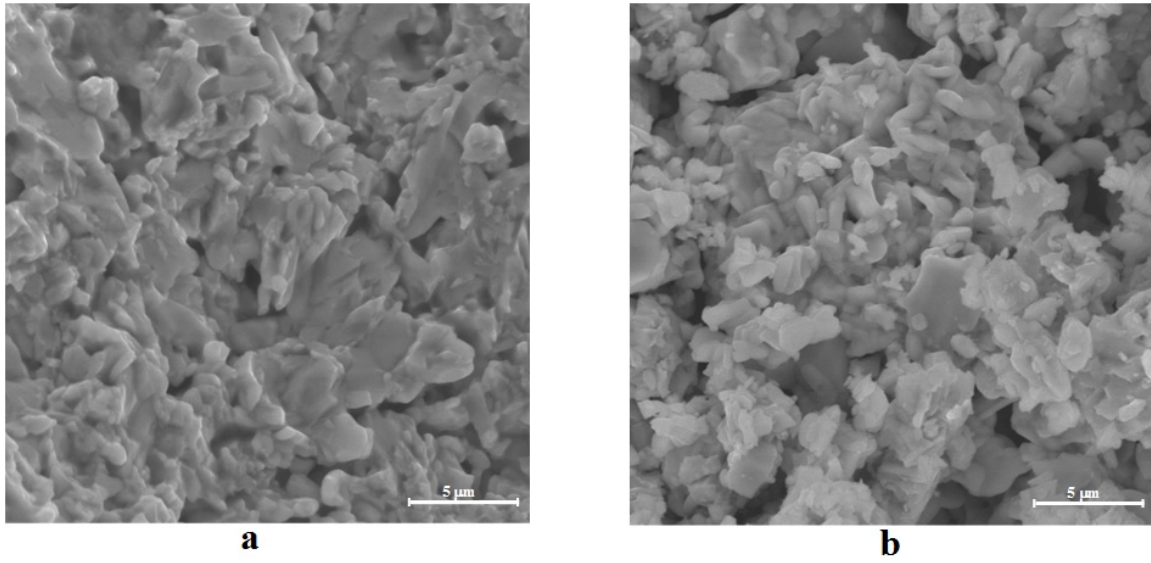


FIG. 4. SEM-images of $(\text{Bi}_{1-x}\text{Sr}_x)_{m+1}\text{Fe}_{m-3}\text{Ti}_3\text{O}_{3(m+1)-\delta}$ ($m = 7$) after its heat treatment at $900\text{ }^\circ\text{C}$: a – un-doped samples; b – Sr-doped samples

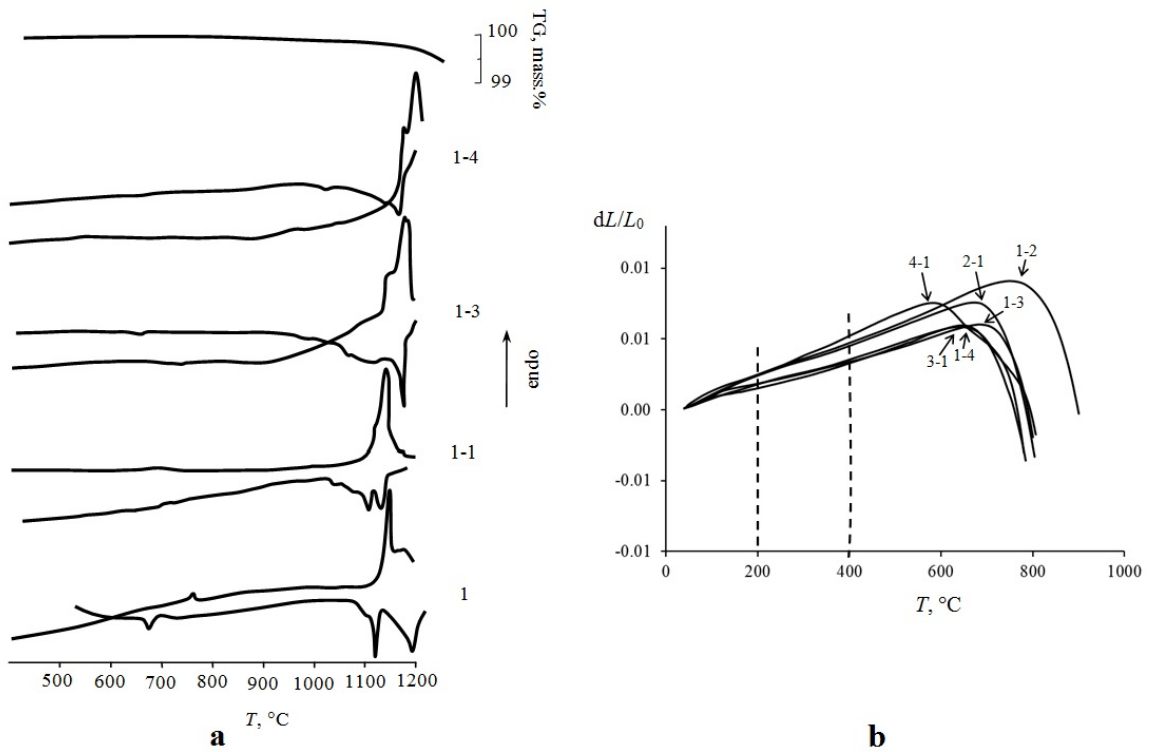


FIG. 5. Thermal analysis: a – DSC and TG curves of $(\text{Bi}_{1-x}\text{Sr}_x)_{m+1}\text{Fe}_{m-3}\text{Ti}_3\text{O}_{3(m+1)-\delta}$ with $m = 4$; b – dilatometric curves of the samples with different m . The curve number corresponds to the sample number (Table 1)

Table 2). A comparison of the obtained α_t with its values for the non-doped Aurivillius phases given in [21] shows that it poorly depends on the degree of isomorphous substitution and the number of layers in the perovskite-like block.

A Mössbauer study has been performed to analyze the effect of isomorphous substitution in the bismuth sublattice on the state of iron ions and on the character of cationic distribution over the structurally nonequivalent octahedral positions in the inner (I) and outer (II) layers of the perovskite-like block. The Mössbauer data for the studied Sr-doped Aurivillius phases with $m = 4 - 7$ are presented in Fig. 6. The spectral parameters for the samples given in Table 3 show that the obtained materials do not contain magnetically ordered phases at room temperature. The isomer shift (IS) and quadrupole splitting (QS) values determined for $(\text{Bi}_{1-x}\text{Sr}_x)_{m+1}\text{Fe}_{m-3}\text{Ti}_3\text{O}_{3(m+1)-\delta}$ ($x = 0 - 0.3$; $m = 4 - 7$), are characteristic for the Fe^{3+} ions in an octahedral environment (see Table 3), that is, the charge compensation at the substitution of Bi^{3+} for Sr^{2+} occurs mainly at the expense of vacancies appearing in the oxygen sublattice. The materials based on the four-layer Aurivillius phase $\text{Bi}_{5-x}\text{Sr}_x\text{FeTi}_3\text{O}_{15-\delta}$ ($x = 0.5, 0.7$) contain a small amount of iron as Fe^{4+} , it being an evidence of the possible charge compensation in presence of high strontium content in the solid solution, and at the expense of the conversion of some Fe^{3+} ions into Fe^{4+} .

TABLE 3. Mössbauer spectral parameters for room temperature samples

	Samples	m	Doublet	Isomer shift, mm/s	Quadrupole splitting, mm/s	Integral intensities ratio, %
1	$\text{Bi}_5\text{FeTi}_3\text{O}_{15}$	4	1	0.37	0.60	76
			2	0.17	0.58	24
1-2	$\text{Bi}_{4.7}\text{Sr}_{0.3}\text{FeTi}_3\text{O}_{15-\delta}$	4	1	0.38	0.60	93
			2	0.20	0.73	12
1-3	$\text{Bi}_{4.5}\text{Sr}_{0.5}\text{FeTi}_3\text{O}_{15-\delta}$	4	1	0.36	0.60	91
			2	-0.02	1.68	9
1-4	$\text{Bi}_{4.3}\text{Sr}_{0.7}\text{FeTi}_3\text{O}_{15-\delta}$	4	1	0.35	0.59	91
			2	0.01	1.72	9
4	$\text{Bi}_8\text{Fe}_4\text{Ti}_3\text{O}_{24}$	7	1	0.38	0.57	73
			2	0.31	0.61	27
4-1	$\text{Bi}_{7.3}\text{Sr}_{0.3}\text{Fe}_4\text{Ti}_3\text{O}_{24-\delta}$	7	1	0.38	0.60	93
			2	0.20	0.73	7

The general shape of the $\text{IS}(m)$ and $\text{QS}(m)$ curves for the non-doped compounds $\text{Bi}_{m+1}\text{Fe}_{m-3}\text{Ti}_3\text{O}_{3(m+1)}$, plotted with an account for the parameters of spectra of iron ions in positions I and II, is described in [6,9,11]. The Sr-doped Aurivillius phases show similar dependences, however with a number of peculiarities. For instance, for the inner layer of the perovskite-like block (I) with the highest concentration of the magnetic ions, the IS value is independent of both m and the degree of isomorphous substitution x . The outer layers of the perovskite-like block (II) in the Aurivillius phases are presumably subjected to structural distortion, and with $m > 5$ significantly differ in the IS and QS values (Fig. 6a,b). This is especially expressed in the Aurivillius phase with $m = 4$, the structure of which contains only 25 % Fe^{3+} ions, which are apparently localized predominantly at the internal positions of the perovskite-like block (Fig. 6). The isomorphous substitution in the bismuth sublattice insignificantly deflects this distribution from the ideal, while for the Aurivillius phases with $m > 5$ this deflection is more apparent. Therefore, the difference between the average charge state and symmetry of the environment of iron ions in positions I and II is more noticeable in solid solutions with $m = 4$ if compared with the phases with $m \geq 5$. The multilayered Aurivillius phases have iron ion content > 40 %, which are apparently distributed less orderly within the perovskite-like block.

The IS values determined for the iron ions in positions I and II converge for the non-doped Aurivillius phases with $m > 5$. The IS value for positions I and II poorly depends on m for the phases $(\text{Bi}_{1-x}\text{Sr}_x)_{m+1}\text{Fe}_{m-3}\text{Ti}_3\text{O}_{3(m+1)-\delta}$ with $x = 0.3$. Apparently, such a degree of bismuth substitution for strontium has no influence on the effective charge of iron ions in the perovskite-like block inner layer and weakly increases the charge in the external layers. As was previously mentioned, the $\text{Bi}_{5-x}\text{Sr}_x\text{FeTi}_3\text{O}_{15-\delta}$ solid solutions ($m = 4$) have a large isomorphous capacity, and the dependence of IS and QS on x is more pronounced in them (see inserts in Fig. 6a,b). It can be seen that the IS and QS values determined for the iron ions in the inner position I, are also independent of x . The greatest difference in the value of the iron ions effective charge is observed for the external position (II) at $x=0.5, 0.7$

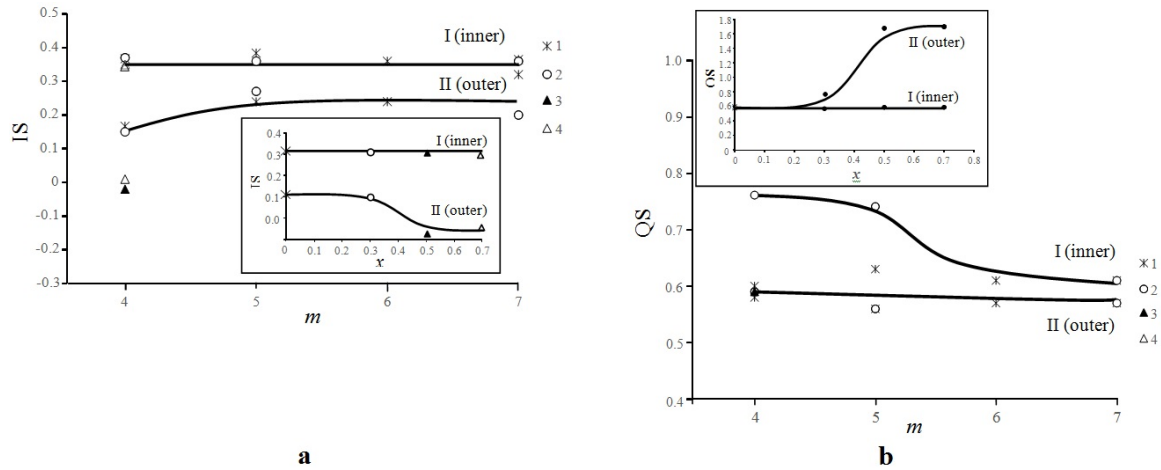


FIG. 6. Mössbauer spectral parameters of $(\text{Bi}_{1-x}\text{Sr}_x)_{m+1}\text{Fe}_{m-3}\text{Ti}_3\text{O}_{3(m+1)-\delta}$: a – the dependence of isomer shift (IS) value on m (insert: the dependence of IS of the Aurivillius phase with $m = 4$ on x); b – the dependence of quadrupole splitting (QS) value on m (insert: the dependence of QS of the Aurivillius phase with $m = 4$ on x). 1 – un-doped Aurivillius phases; 2 – Sr-doped Aurivillius phases with $m = 4 - 7$, $x = 0.3$; 3 – Sr-doped Aurivillius phases with $m = 4$, $x = 0.5$; 4 – Sr-doped Aurivillius phases with $m = 4$, $x = 0.7$

(see insert in Fig. 6a), which is accompanied by an increase in the symmetry of their environment (see insert in Fig. 6b). Apparently, this may indicate the dominating localization of strontium atoms in the outer layers of the perovskite-like block.

The results of magnetic measurements of the obtained materials are shown in Figs. 7,8 (for the samples' composition, see Table 1). It can be seen that at 5 K, the samples have a pronounced dependence of the $M(H)$ magnetization curves shape on m . For the samples with $m > 5$, regardless of the degree of isomorphous substitution, there is a deviation from linearity that decreases with the increasing h . It should be noted that even at low temperatures and very large fields, magnetic saturation is not achieved. For the Aurivillius phases with $m > 5$, the $M(H)$ dependences are close to linear. At $T = 5$ K, the hysteresis loops are absent in all samples, which can indicate their paramagnetic state at any temperature, however a noticeable deviation from linearity for the compounds with $m \leq 5$ suggests that this is not true, at least for these samples. When the temperature increases up to 300 K, all the $M(H)$ dependences become linear. At 300 K, the magnitude of the Aurivillius phase's magnetic moment obtained in the present work, as well as of those described in [14], is 0.1 – 0.2 emu/g at 20 kOe (see Table 2). As can be seen, the essential differences in their composition and, correspondingly, the differences in the Fe^{3+} magnetic ion content in the structure, practically do not affect the value of M near room temperature.

Figure 8a shows the temperature dependences of the specific magnetization $M(T)$, the shape of which is typical for paramagnets. The values of the magnetic responses differ significantly in this case. For instance, the Aurivillius phases with $m = 7$ have approximately four-fold less magnetization at $T = 5$ K than the phases with $m = 4$. However, the analysis performed on the reverse temperature dependences of the magnetization $1/M(T)$ (Fig. 8b) shows that it is impossible to isolate a linear section, that is, it is impossible to accurately describe the obtained curves by the Curie-Weiss law.

Nevertheless, it is possible to note their similarity, from which only the $m = 7$ Aurivillius phases sharply deviate. The violation of the strictly paramagnetic behavior can be due to the presence of a magnetically ordered state or, more likely, magnetic fluctuations. Although a number of studies have reported that $\text{Bi}_5\text{Ti}_3\text{FeO}_{15}$ ($m = 4$) demonstrates paramagnetic behavior without the long-range magnetic order up to very low temperatures [16,26], there are indications of the appearance of an antiferromagnetic transition in the 50 – 80 K range. A theoretical analysis of [12] shows that the magnetic behavior of the given compound can be described as a short-range (localized) antiferromagnetic interaction, which confirms the assumption made.

According to Mössbauer data, the magnetic ions of the non-doped and Sr-doped Aurivillius phases with $m < 5$ are distributed over the perovskite-like block more orderly. Magnetometric results show the greatest deviation from paramagnetic behavior particularly for these samples. Taking into account the fact that the exchange interaction is most strongly manifested in the nearest magnetic ion neighbors, it can be concluded that in the case when antiferromagnetic fluctuations exist in the system, they should be localized predominantly inside these blocks.

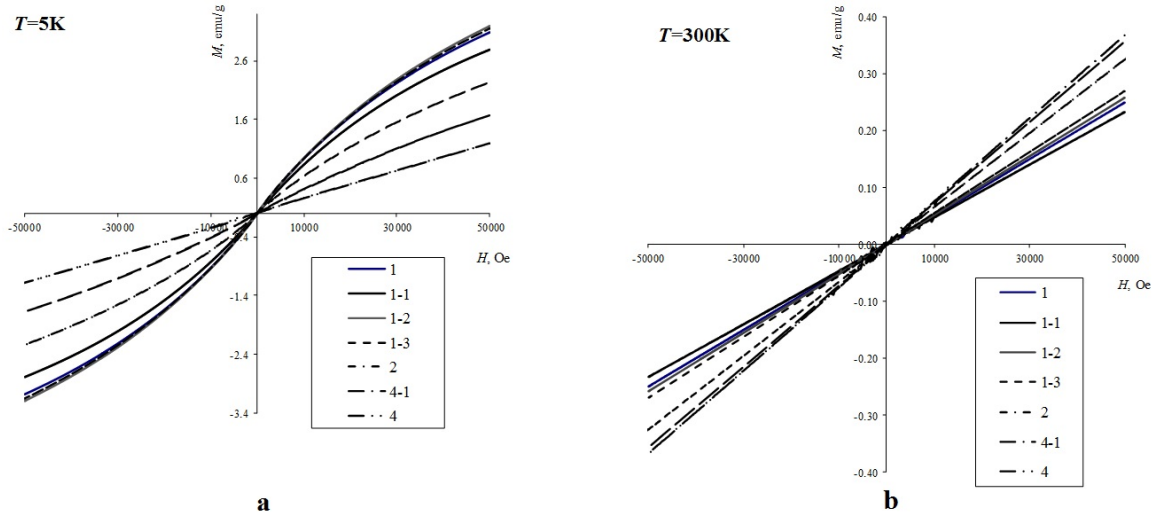


FIG. 7. Magnetization curves of $(\text{Bi}_{1-x}\text{Sr}_x)_{m+1}\text{Fe}_{m-3}\text{Ti}_3\text{O}_{3(m+1)-\delta}$ measured at 2K (a) and 300K (b). The curve number corresponds to the sample number (Table 1)

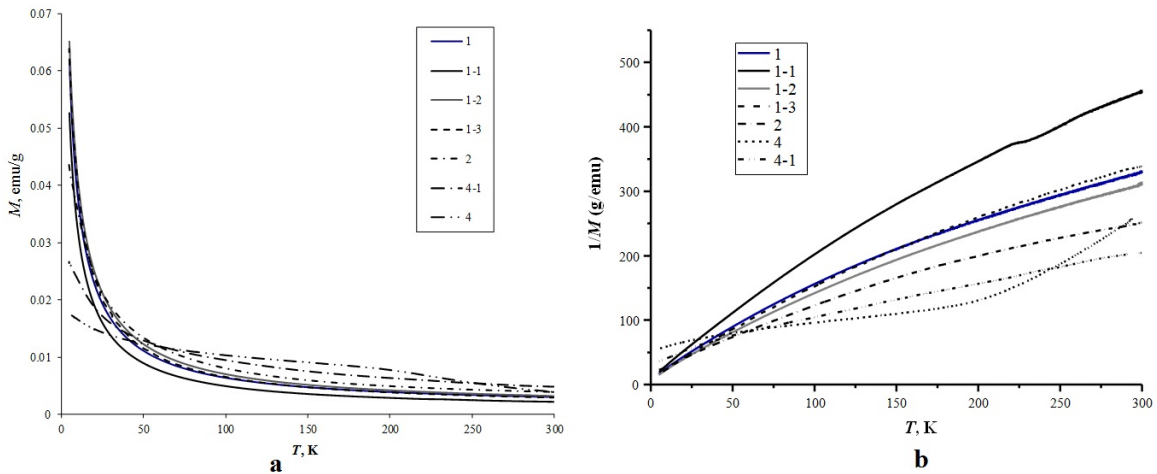


FIG. 8. Temperature dependences of inverse magnetization (a) and inverse magnetization (b) of $(\text{Bi}_{1-x}\text{Sr}_x)_{m+1}\text{Fe}_{m-3}\text{Ti}_3\text{O}_{3(m+1)-\delta}$. The curve number corresponds to the sample number (Table 1)

Thus, the magnetic characteristics of the structures based on the Sr-doped Aurivillius phases have been obtained and found to be associated with the presence of a paramagnetic system formed by the magnetic moments of iron ions, between which, there exists an exchange interaction of the antiferromagnetic type. The features of the magnetic behavior of these phases can be presumably explained by magnetic fluctuations.

4. Conclusions

The features of the solid-phase formation of the layered perovskite-like oxides of the Aurivillius phase type $(\text{Bi}_{1-x}\text{Sr}_x)_{m+1}\text{Fe}_{m-3}\text{Ti}_3\text{O}_{3(m+1)-\delta}$ ($x = 0.0 - 0.7$; $m = 4 - 7$) with a perovskite-like block $\approx 2 - 3$ nm thick have been described. The optimal conditions for the production of ceramic-based materials have been determined. The degree of isomorphous substitution in the bismuth sublattice was found to decrease along with the increase of m and, accordingly, of h . The formation of a layered perovskite-like structure of the Aurivillius phases with a predetermined stoichiometry occurs with a gradual increase of m , while at $m > 5$ and $h > 2$ nm, isomorphous substitution leads to an increasing amount of impurities in the reaction system.

Thermal analysis data showed that the temperature for the initiation of materials decomposition gradually decreases along with the increasing m , and the Curie point and the sintering onset temperature are in one temperature domain.

The results of the Mössbauer and magnetometric studies made it possible to make an assumption that the magnetic ions in the internal positions of a perovskite-like block are engaged in an antiferromagnetic-type exchange interaction that affects the magnetic properties of the studied materials. The effect of isomorphous substitution in the bismuth sublattice on the nature of the iron ions distribution and the magnetic behavior of the Aurivillius phases is less pronounced. The features of the magnetic behavior of the obtained materials can be presumably explained by magnetic fluctuations.

Acknowledgement

This work was financially supported by the Russian Foundation for Basic Research (Grant No. 16-03-01056).

References

- [1] Keeney L., Downing C., Schmidt M., Pemble M.E., Nicolosi V., Whatmore R.W. Direct atomic scale determination of magnetic ion partition in a room temperature multiferroic material. *Sci. Rep.*, 2017, **7**(1), P. 1737–1748.
- [2] Faraz A., Maity T., Schmidt M., Deepak N., Roy S., Pemble M.E., Whatmore R.W., Keeney L. Direct visualization of magnetic-field-induced magnetoelectric switching in multiferroic Aurivillius phase thin films. *J. Am. Cer. Soc.*, 2017, **100**(3), P. 975–987.
- [3] Keeney L., Maity T., Schmidt M., Amann A., Deepak N., Petkov N., Roy S., Pemble M. E., Whatmore R. W. Magnetic field-Induced ferroelectric switching in multiferroic Aurivillius phase thin films at room temperature. *J. Am. Ceram. Soc.*, 2013, **96**(8), P. 2339–2357.
- [4] Varentsova A.S., Potkina M.N., von Malottki S., Heinze S., Bessarab P.F. Interplay between size and stability of magnetic skyrmions. *Nanosystems: Phys. Chem. Math.*, 2018, **9**(3), P. 356–363.
- [5] Lomanova N.A., Gusarov V.V. On the limiting thickness of the perovskite-like block in the Aurivillius phases in the $\text{Bi}_2\text{O}_3\text{-TiO}_2\text{-Fe}_2\text{O}_3$ system. *Nanosystems: Phys. Chem. Math.*, 2011, **2**(3), P. 93–101.
- [6] Lomanova N.A., Semenov V.G., Panchuk V.V., Gusarov V.V. Structural changes in the homologous series of the Aurivillius phases $\text{Bi}_{n+1}\text{Fe}_{n-3}\text{Ti}_3\text{O}_{3n+3}$. *J. Alloys Comp.*, 2012, **528**, P. 103–108.
- [7] Aurivillius B. Mixed bismuth oxides with layer lattices. I. *Ark. Kemi.*, 1949, **1**(1), P. 463–471.
- [8] Sosnowska I., Peterlin-Neumaier T., Steichele E.J. Spiral magnetic ordering in bismuth ferrite. *Phys. C: Solid State Phys.*, 1982, **15**, P. 4835–4846.
- [9] Lomanova N.A., Semenov V.G., Panchuk V.V., Gusarov V.V. Structural features and stability of the Aurivillius phases $\text{Bi}_{n+1}\text{Fe}_{n-3}\text{Ti}_3\text{O}_{3n+3}$. *Dokl. Chem.*, 2012, **447**(2), P. 293–295.
- [10] Lomanova N.A., Morozov M.I., Ugolkov V.L., Gusarov V.V. Properties of Aurivillius phases in the $\text{Bi}_4\text{Ti}_3\text{O}_{12}\text{-BiFeO}_3$ system. *Inorganic Materials*, 2006, **42**(2), P. 189–195.
- [11] Jartych E., Gaska K., Przewoznik J., Kapusta C., Lisinska-Czekaj A., Czekaj D., Surowiec Z. Hyperfine interactions and irreversible magnetic behavior in multiferroic Aurivillius compounds. *Nukleonika*, 2013, **58**, P. 47–51.
- [12] Birenbaum A.Y., Ederer C. Potentially multiferroic Aurivillius phase $\text{Bi}_5\text{FeTi}_3\text{O}_{15}$: cation site preference, electric polarization, and magnetic coupling from first principles. *Phys. Rev. B*, 2014, **90**, P. 214109–214121.
- [13] Lomanova N.A., Gusarov V.V. Impedance spectroscopy of polycrystalline materials based on the Aurivillius phase system $\text{Bi}_4\text{Ti}_3\text{O}_{12}\text{-BiFeO}_3$. *Nanosystems: Phys. Chem. Math.*, 2012, **3**(6), P. 112–122.
- [14] Lomanova N.A., Pleshakov I.V., Volkov M.P., Gusarov V.V. Magnetic properties of Aurivillius phases $\text{Bi}_{m+1}\text{Fe}_{m-3}\text{Ti}_3\text{O}_{3m+3}$ with $m=5, 5.5, 7, 8$. *Mat. Sci. Eng. B*, 2016, **214**, P. 51–56.
- [15] Huang Y., Wang G., Sun Sh., Wang J., Peng R., Lin Y., Zhai X., Fu Zh., Lu Y.. Observation of exchange anisotropy in single-phase layer structured oxides with long periods. *Sci. Rep.*, 2015, **5**, P. 15261–15266.
- [16] Pikula T., Dzik J., Guzdek P., Mitsuik V.I., Surowiec Z., Panek R., Jartych E. Magnetic properties and magnetoelectric coupling enhancement in $\text{Bi}_5\text{Ti}_3\text{FeO}_{15}$ ceramics. *Ceram. Int.*, 2017, **43**(14), P. 11442–11449.
- [17] Lomanova N.A., Pleshakov I.V., Volkov M.P., Gusarov V.V. The thermal behavior of mixed-layer Aurivillius phase $\text{Bi}_{13}\text{Fe}_5\text{Ti}_6\text{O}_{39}$. *J. Therm. Anal. Calorim.*, 2018, **131**, P. 473–478.
- [18] Lomanova N.A., Tomkovich M.V., Ugolkov V.L., Gusarov V.V. Formation and thermal properties of nanocrystalline $\text{Bi}_4\text{Ti}_3\text{O}_{12}$. *Russ. J. Appl. Chem.*, 2017, **90**(6), P. 831–837.
- [19] Lomanova N.A., Ugolkov V.L., Panchuk V.V., Semenov V.G. Formation and thermal behaviors of the Aurivillius phases $\text{A}_{m-1}\text{Bi}_2\text{Fe}_{m-3}\text{Ti}_3\text{O}_{3m+3-\delta}$ (A-Bi, Sr). *Russ. J. Gen. Chem.*, 2017, **87**(3), P. 365–372.
- [20] Lomanova N.A., Gusarov V.V. Phase states in the $\text{Bi}_4\text{Ti}_3\text{O}_{12}\text{-BiFeO}_3$ section in the $\text{Bi}_2\text{O}_3\text{-TiO}_2\text{-Fe}_2\text{O}_3$ system. *Russ. J. Inorg. Chem.*, 2011, **56**(4), P. 616–620.
- [21] Lomanova N.A., Ugolkov V.L., Gusarov V.V. Thermal behavior of layered perovskite-like compounds in the $\text{Bi}_4\text{Ti}_3\text{O}_{12}\text{-BiFeO}_3$ system. *Glass Physics and Chemistry*, 2007, **33**(6), P. 608–612.
- [22] Isupov V.A. Curie Temperatures of $\text{A}_{m-1}\text{Bi}_2\text{M}_m\text{O}_{3m+3}$ layered ferroelectrics. *Inorganic Materials*, 1997, **33**(9), P. 1106–1110.
- [23] Snedden A., Hervoche Ch. H., Lightfoot Ph. Ferroelectric phase transition in $\text{SrBi}_2\text{Nb}_2\text{O}_9$ and $\text{Bi}_5\text{Ti}_3\text{FeO}_{15}$: a powder neutron diffraction study. *Phys. Rev.*, 2003, **67**, P. 092102–092105.
- [24] Krzhizhanovskaya M., Filatov S., Gusarov V., Paufler P., Bubnova R., Morozov M., Meyer D.C. Aurivillius phases in the $\text{Bi}_4\text{Ti}_3\text{O}_{12}\text{-BiFeO}_3$ system: thermal behaviour and crystal structure. *Z. Anorg. Allg. Chem.*, 2005, **631**, P. 1603–1608.
- [25] Yang J., Tong W., Liu Z., Zhu X.B., Dai J.M., Song W.H., Yang Z. R., Sun Y.P. Structural, magnetic, and EPR studies of the Aurivillius phase $\text{Bi}_6\text{Fe}_2\text{Ti}_3\text{O}_{18}$ and $\text{Bi}_6\text{FeCrTi}_3\text{O}_{18}$. *Phys. Rev. B*, 2012, **86**, P. 104410–104417.
- [26] Dong X.W., Wang K.F., Wan J.G., Zhu J.S., Liu J.-M. Magnetocapacitance of polycrystalline $\text{Bi}_5\text{Ti}_3\text{FeO}_{15}$ prepared by sol-gel method. *J. Appl. Phys.*, 2008, **103**, P. 0941010–0941014.
- [27] Morozov M.I., Mezentseva L.P., Gusarov V.V. Mechanism of formation of $\text{Bi}_4\text{Ti}_3\text{O}_{12}$. *Russ. J. Gen. Chem.*, 2002, **72**(7), P. 1038–1040.
- [28] Morozov M.I., Gusarov V.V. Synthesis of $\text{A}_{m-1}\text{Bi}_2\text{M}_m\text{O}_{3m+3}$ compounds in the $\text{Bi}_4\text{Ti}_3\text{O}_{12}\text{-BiFeO}_3$ system. *Inorganic Matials*, 2002, **38**(7), P. 723–729.

- [29] Lomanova N.A., Tomkovich M.V., Sokolov V.V., Gusarov V.V. Special features of formation of nanocrystalline BiFeO₃ via the glycine-nitrate combustion method. *Russ. J. Gen. Chem.*, 2016, **86**(10), P. 2256–2262.
- [30] Proskurina O.V., Tomkovich M.V., Bachina A.K., Sokolov V.V., Danilovich D.P., Panchuk V.V., Semenov V.G., Gusarov V.V. Formation of nanocrystalline BiFeO₃ under hydrothermal conditions. *Russ. J. Gen. Chem.*, 2017, **87**(11), P. 2507–2515.
- [31] Dubey S., Subohi O., Kurchania R. Optimization of calcination and sintering temperature of sol-gel synthesised Ba₂Bi₄Ti₅O₁₈, Pb₂Bi₄Ti₅O₁₈ and Sr₂Bi₄Ti₅O₁₈ ceramics. *Ceram. Int.*, 2017, **43**(15), P. 12755–12763.
- [32] Lomanova N.A., Gusarov V.V. Effect of the phase composition of the starting mixture on the formation of the layered perovskite-like compound Bi₇Fe₃Ti₃O₂₁. *Russ. J. Inorg. Chem.*, 2010, **55**(10), P. 1541–1545.
- [33] Lomanova N.A., Gusarov V.V. Effect of surface melting on the formation and growth of nanocrystals in the Bi₂O₃–Fe₂O₃ system. *Russ. J. Gen. Chem.*, 2013, **83**, P. 2251–2253.
- [34] Tugova E.A., Travitskov A.V., Tomkovich M.V., Sokolov V.V., Nenasheva E.A. Solid -phase synthesis and dielectric properties of materials based on LaAlO₃–CaTiO₃ system. *Russ. J. Appl. Chem.*, 2017, **90**(11), P. 1738–1745.
- [35] Tugova E.A. New DySrAlO₄ compound synthesis and formation process correlations for LnSrAlO₄ (Ln - Nd, Gd, Dy) series. *Acta Metallurgica Sinica (English Letters)*, 2016, **29**(5), P. 450–456.
- [36] Popkov V.I., Tugova E.A., Bachina A.K., Almyasheva O.V. The formation of nanocrystalline orthoferrites of rare-earth elements XFeO₃ (X -Y, La, Gd) via heat treatment of coprecipitated hydroxides. *Russ. J. Gen. Chem.*, 2017, **87**(11), P. 2516–2524.
- [37] Ostroushko A.A., Russkikh O.V. Oxide material synthesis by combustion of organic-inorganic. *Nanosystems: Phys. Chem. Math.*, 2017, **8**(4), P. 476–502.
- [38] Tugova E., Yastrebov S., Karpov O., Smith R. NdFeO₃ nanocrystals under glycine-nitrate combustion formation. *J. Cryst. Grow.*, 2017, **467**, P. 88–92.
- [39] Morozov M.I., Lomanova N.A., Gusarov V.V. Specific Features of BiFeO₃ formation in a mixture of bismuth(III) and iron(III) oxides. *Russ. J. Gen. Chem.*, 2003, **73**, P. 1772–1776.
- [40] Bespalova Zh.I., Khramenkova A.V. The use of transient electrolysis in the technology of oxide composite nanostructured materials: review. *Nanosystems: Phys. Chem. Math.*, 2016, **7**(3), P. 433–450.
- [41] Gusarov V.V., Suvorov S.A. Melting-point of locally equilibrium surface phases in polycrystalline systems based on a single volume phase. *Russ. J. Appl. Chem.*, 1990, **63**(8), P. 1479–1484.
- [42] Gusarov V.V. The thermal effect of melting in polycrystalline systems. *Thermochimica Acta*, 1995, **256**(2), P. 467–472.
- [43] Gusarov V.V. Fast Solid-Phase Chemical Reactions. *Russ. J. Gen. Chem.*, 1997, **67**(12), P. 1846.
- [44] Shannon R.D., Prewitt C.T. Effective ionic radii in oxides and fluorides. *Acta Crystallogr. B.*, 1969, **25**(6), P. 928–929.